applied optics

Distribution model of the surface roughness in magnetorheological jet polishing

Kuo Hai,[1,2] Longxiang Li,[1,2,*] Haixiang Hu,[1] Zhiyu Zhang,[1] Yang Bai,[1] Xiao Luo,[1] Liqi Yi,[1,2] Xi Yang,[1,2] Donglin Xue,[1] and Xuejun Zhang[1]

[1]Key Laboratory of Optical System Advanced Manufacturing Technology, Changchun Institute of Optics, Fine Mechanics and Physics, Chinese Academy of Sciences, Changchun, Jilin 130033, China
[2]University of Chinese Academy of Sciences, Beijing 100049, China
*Corresponding author: leellxhit@126.com

Received 18 June 2020; revised 27 August 2020; accepted 2 September 2020; posted 3 September 2020 (Doc. ID 400464); published 28 September 2020

Magnetorheological jet polishing (MJP) plays an important role in polishing complex cavities and special optical elements with high precision. However, the roughness distribution function that describes the variation with polishing time of the roughness value of every area in the polishing area has not been studied deeply. In this paper, the influence of the roughness distribution on the removal function of MJP in optics (with a roughness of less than 10 nm) and its evolution model in the spatial and time domains are studied. With the increase of polishing time, the surface roughness of the central area linearly increases, forming surface defects, such as pits. The roughness of the polishing area exhibits a limited growth trend. Verification experiments are carried out on BK7 glass. The results of the roughness distribution on the removal function prove the correctness of the model. The model laid a foundation; therefore, it has important guidance and reference value for the application to the whole aperture polishing.

https://doi.org/10.1364/AO.400464

1. INTRODUCTION

Advanced optical designs often require shapes and materials that are challenging to polish [1,2]. Particularly, conformal, freeform, and steep concave optics are more difficult or impossible to finish using conventional techniques due to mechanical interferences and steep local slopes [3]. Magnetorheological jet polishing (MJP) plays an important role in polishing these optics with high precision [3–6].

The manufacturing process of precision optical components not only requires the polishing tool to correct the surface shape of the workpiece [1–7], but also needs to ensure that the surface shape achieves a low microroughness [8–11].

As for the MJP technology, many research teams have studied the removal model and optical surfacing technology. Kordonski *et al.* [1–4] studied MJP's basic principles and found that its removal has an M-shaped profile. Kim *et al.* developed the theoretical models for the prediction of material removal by using the conventional wear model and granular flow theory [7]. Tan Wang *et al.* studied the basic polishing principles, introduced and analyzed four main polishing models using an integrated polishing tool, and designed a special machining track to control midspatial frequency errors [12,13]. Zhang *et al.* [14] and Tan Wang [15] corrected the surface error using the rotational footprint so that the W-shaped removal function became a Gaussian-like removal function. Yang designed a bevel-cut-like tool influence function to polish thin rolled edges [16].

While the existing research on removal function and optical surfacing in MJP has been extensive, those on surface roughness are relatively few. There are two main aspects of surface roughness research in existing literature.

On the one hand, some literature has tested the final surface roughness of the workpiece after the MJP process, illustrating that the MJP technology has the ability to reduce the final roughness [1–3,7,12–15]. However, the amount of work involved in measuring the roughness value of each point on the workpiece is huge and does not conform to the actual figuring process. In some applications, optical elements require a consistent value of the roughness at all points. For example, when there are some points on the surface of a high laser reflective element, the roughness of these points is large, and the result will be that the reflectivity of these points is reduced, the scattering energy is large, and the temperature of these points of the area will increase, which will eventually cause damage to the entire reflective element. In such a conclusion, the roughness is taken as an index to measure the MJP technology to judge the merits and demerits of this technology. Moreover, their study on the roughness is the final value of the roughness of the workpiece surface after polishing, while the roughness distribution model we studied is a dynamic model due to the introduction of time variables.

On the other hand, literature about abrasive jet polishing conducted the impact energy, impact angle, and other influences o n t he s urface r oughness, q uantified th e damage from single impacting articles, and used the results to improve the analytical model of roughness and erosion rate [17–20]. In this kind of research, the conditions that affect the roughness (such as particle size, collision velocity and energy) in the polishing process are studied, and the influence of each index on the roughness is quantitatively given. However, this is also a static model, with no time variables. When the set of process parameters is fixed but the polishing time is different, the roughness obtained after polishing is different, which cannot be concluded in other models. Due to the introduction of time variables, our roughness model can predict the same results as the experiment, so the time term should not be ignored. Hence, the surface distribution model is deemed to be more persuasive than the traditional roughness model.

Different from abrasive jet polishing, the MJP removal mechanism includes not only the impacting effect, but also the shearing effect, but it is dominated by shearing in the removal of material [2,7,12]. These two modes of action have different effects on the roughness. In polished areas, the ratio of impacting and shearing is different for each point of removal and cannot be described by a single polishing mechanism which can be proved in Kim's research [7]. It illustrated that the roughness value was different at the center, the area of deepest erosion, and the edge of the axisymmetric spot in the removal area after polishing. In the fixed-point removal function region, the distribution of the roughness is uneven. It is conceivable that when using such a removal function to polish the whole aperture surface, the final roughness distribution will be uneven, which will further affect the imaging quality of the optical instrument. Therefore, it is worthwhile to research and consider the roughness distribution rule in the removal function region.

Different from the previous studies, the roughness distribution model proposed in this paper is a function of three-dimensional coordinates and time. It is not only related to the polishing time, but also to the specific position within the removal function during polishing, and to the initial roughness of the surface. In this paper, we use the roughness distribution function to describe the variation of the roughness value of different regions with the polishing time, which can more clearly describe the variation rule of the roughness of each point and improve the analytical model of roughness to better match the experimental results.

2. COMPUTATIONAL FLUID DYNAMICS THEORY AND SIMULATION

A. Classical Removal Theory

For the classical removal principle of MJP, a large amount of literature has been studied, and the removal function model has been given. The removal model can be simulated using the Preston's classical expression by the following equation [2,7,12,16]:

$$\frac{dR}{dt} = kpv = k\frac{F}{\mu S}v = k\frac{\tau v}{\mu}, \tag{1}$$

where dR/dt is the material removal rate, k is a nondimensional constant that is influenced by material properties, temperature, and other experimental parameters, p is the normal pressure acting on the surface, and v is the shear velocity of the MR fluid on the workpiece surface. S is the surface area on which wear occurs, F is the frictional force between the glass and the pitch, μ is the coefficient of friction, and τ is the surface shear stress.

While surface roughness is considered to be a measure of finely spaced surface irregularities, it is also a result of uneven microscopic removal. By analogy with the removal function, the influence of pressure and velocity factors on the roughness change can be analyzed, and then the influence of impact process and shear process, respectively, on the roughness value of each point in the removal function area is studied. Therefore, the roughness distribution will be analyzed from the pressure and velocity of the fluid on the workpiece surface.

According to the Preston equation, the macroscopic factors that have an impact on the material removal effect are velocity and pressure, which will affect the distribution of removal efficiency at each point, which can be concluded from previous literature. Both of these are directly proportional to the material removal rate, and they are position-related functions that do not change with time [12]. While surface roughness is considered to be a measure of finely spaced surface irregularities, it is also a result of uneven microscopic removal. By analogy with the removal function, the influence of pressure and velocity factors on the roughness change can be analyzed, and then the influence of the impact process and shear process, respectively, on the roughness value of each point in the removal function area is studied. Therefore, the roughness distribution will be analyzed from the pressure and velocity of the fluid on the workpiece surface.

B. Distribution Model of Velocity and Pressure

To more clearly and accurately describe the process of material removal in MJP, the pressure and velocity parameters require further analysis. The conventional and accurate method is to use fluid dynamics theory for finite element analysis [7,12,16].

A large amount of literature has described the characteristics of magnetorheological (MR) jet beams [1–7,12,16,21], which is characterized by smooth and orderly execution. When the MR fluid passes through a magnetic field, the MR effect occurs in the MR fluid. By increasing the viscosity, the destruction of the efflux structure caused by the disturbance can be restrained, a stable and smooth cylindrical liquid can be transmitted in the air, and its initial state can be maintained at a long distance [1–7,22]. MR fluid is a fluid in which the energy dissipation rate is low, and the distance is insensitive compared to that of liquid fluid [21]. In the transmission process of MR fluid, the shear-stress transport $k-\omega$ model can be used to describe the characteristics of the abrasives and the laminar flow transition process from the nozzle to the wall surface processing in the turbulent form [23,24]. The basic model of $k-\omega$ is as follows:

Kinematic Eddy Viscosity:

$$\nu_T = \frac{k}{\omega}, \tag{2}$$

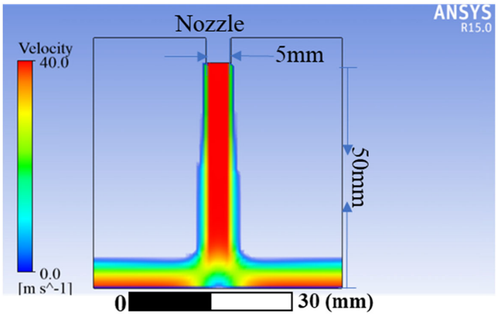

Fig. 1. Simulation of the MR jet flow process by CFD.

Turbulent Kinetic Energy:

$$\frac{\partial k}{\partial t}+U_j\frac{\partial k}{\partial x_j}=\tau_{ij}\frac{\partial U_i}{\partial x_j}-\beta^* k\omega+\frac{\partial}{\partial x_j}\left[(\nu+\sigma^*\nu_T)\frac{\partial k}{\partial x_j}\right], \quad (3)$$

Specific Dissipation Rate:

$$\frac{\partial \omega}{\partial t}+U_j\frac{\partial \omega}{\partial x_j}=\alpha\frac{\omega}{k}\tau_{ij}\frac{\partial U_i}{\partial x_j}-\beta\omega^2+\frac{\partial}{\partial x_j}\left[(\nu+\sigma\nu_T)\frac{\partial \omega}{\partial x_j}\right], \quad (4)$$

where v, k, and ω, are the turbulent viscosity, kinetic, and turbulent kinetic energy dissipation rate, respectively, U_j is the particle velocity, $\alpha = 0.52$, $\beta_0 = 0.072$, $\beta_0^* = 0.09$, $\sigma = \sigma^* = 0.5$ are the initial values of each parameter, and other coefficients are constant.

To display the calculation results more intuitively and to conduct a detailed study on the flow structure, the commercial CFD software was used to simulate the MJP process, so that pressure and velocity distributions could be analyzed more intuitively and accurately [25,26]. The turbulence model and its parameters were input into the CFD simulation.

Figure 1 shows the flow process of the MR fluid from the nozzle to the workpiece surface. The other initial parameters and boundary conditions were the nozzle diameter of 5 mm, the processing distance of 50 mm, and inlet type is velocity-inlet with the fluid initial velocity of 40 m/s, and the initial gauge pressure is 1 MPa. The workpiece type is the wall with no slip. In the process of MJP, the particle size of the abrasive used was less than or equal to one micron. Due to the large liquid viscosity, the abrasive was considered to be consistent with the movement state of the iron powder carrying it for subsequent simulation. According to the analysis in the literature [12–16], the velocity and pressure distribution are characterized by rotational symmetry, hence the CFD simulation was carried out in the plane with the workpiece diameter as the y axis and the processing distance as the x axis to transform the problem into a two-dimensional problem.

The pressure volume rendering shows that in Fig. 2, the normal pressure on the workpiece decreases rapidly outward from the impact center, and the effective range of pressure in the workpiece is about 20 mm. In the area near the wall, as shown in Fig. 2, the abrasive shear velocity increased from the impact center.

In the effective range of the pressure, the materials can be removed as a matter of a fact. In the removal area, the shear

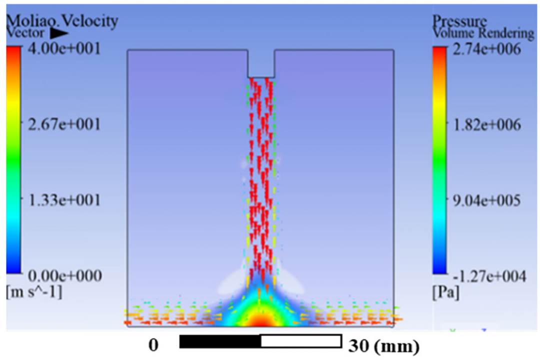

Fig. 2. Simulation results of velocity and pressure distribution.

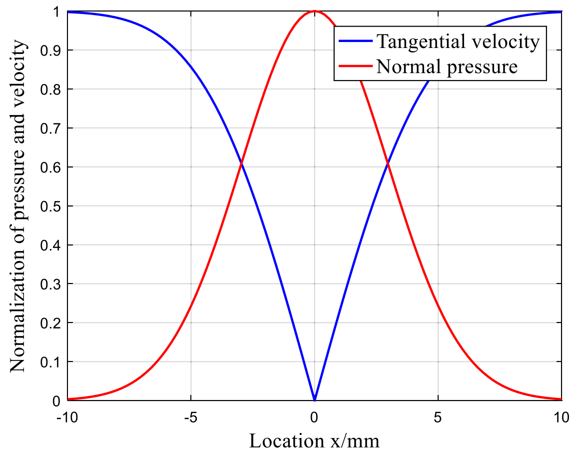

Fig. 3. Axial approximate normalized velocity and pressure simulation curve.

velocity of the fluid remained basically unchanged after increasing to the maximum value. The simulation result of axial approximate normalized velocity and pressure curve is shown in Fig. 3. As seen from Fig. 3, when the fluid impinges on the surface of the workpiece, the central pressure is the maximum, while the velocity is the minimum at this time. The material removal mainly depends on the pressure, which is removed by impact, the removal mechanism is similar to ion beam finishing (IBF) [27,28]. When the tangential velocity of the fluid increases and the normal pressure on the surface decreases, the removal of the material depends on the combined action of normal pressure and tangential velocity. This shear action can remove a large number of materials; the removal mechanism is similar to magnetorheological finishing (MRF) [29,30].

Through the theory of fracture mechanics, the critical normal and critical shear forces indicate the critical force required to remove the material on the surface[12]. And the critical normal force is larger than the critical shear force, hence the removal of material by shear action is essential.

From the velocity vector of the CFD simulation, the impact and shear actions exist throughout the removed area. Due to the different distribution values of pressure and velocity, the two forms of action occupy different proportions in different locations. For the convenience of analysis, the acting area dominated by shear action is called polishing area, and the acting area

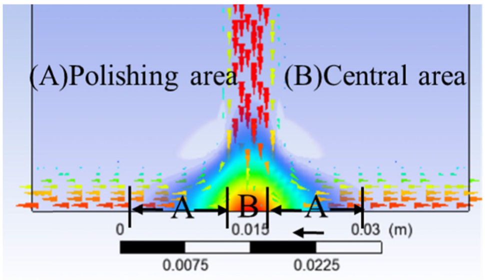

Fig. 4. Division of the action area between the fluid and workpiece.

dominated by impact action is called the central area, as shown in Fig. 4. The central area is the fluid impacting area, and in the polishing area the fluid flows along the surface. The influence of these two actions on the roughness distribution pattern will be analyzed below.

3. MODELING OF THE SURFACE ROUGHNESS DISTRIBUTION

A. Influence of Impact Action on the Change of Roughness

Although the shear velocity of the fluid and the pressure of the fluid on the workpiece surface influence the removal rate of the material, their removal effects on the microscopic morphology of the material are completely different. In combination with their distribution rules, the effects of velocity and pressure on roughness are discussed below.

In the impact process of the MR fluid to the workpiece, through the theory of fracture mechanics, to make the material removal the normal pressure should be greater than the critical force (Pcr) of the surface [12]. The formula for calculating the critical load of a material fracture is given by Eq. (5) [31]:

$$Pcr = 2 \times 10^5 ({K_{IC}}^4 / {H_N}^3), \tag{5}$$

where Pcr is the critical load of the material fracture, K_{IC} is the fracture toughness of materials, and H_N is the material hardness.

For the BK7 glass, $K_{IC} = 0.86\,\mathrm{MPa{\cdot}m^{1/2}}$ and $H_N = 5.2\,\mathrm{GPa}$, hence Pcr results in a force of 0.78 N. When MR jet polishing process, the maximum velocity is 40 m/s, and the interaction time between abrasive particles and the surface is Δt, which can be obtained from the theory of particle forces described by Van Haarlem [32]. The movement of abrasive particles satisfies the momentum equation, and the pressure calculated by the equation is lower than the Pcr. That means the impact action does not remove the material that is different from the actual performance when polishing a longer time. It is not suitable for studying the variation of roughness.

The microscopic removal process of materials cannot be calculated simply. In the process of MJP, as shown in Figs. 5(a) and 5(b), the initial momentum and energy of the fluid jet impact are not enough to break the material, but these impacts have a positive effect on the material removal for the subsequent impact of multiple particles. After the accumulation of overlapping impacting processes, the affected area becomes fatigued and loosened, and the fracture limit (K_{IC}) of the material subsequently decreases, as shown in Fig. 5(c). The pressure provided

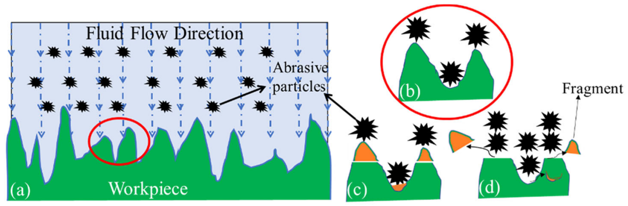

Fig. 5. Material removal process in fluid impacting.

by the particles can reach the new fracture limit of the material, allowing the surface material to be removed, as shown in Fig. 5(d).

In other literature of the impact action to roughness, Slikkerveer *et al.* [33] studied the roughness model in the abrasive jet micromachining (AJM), and the results implied that the surface roughness was only a function of the particle kinetic energy due to the velocity component perpendicular to the surface, and was independent of particle size. And the result is consistent with the observations of Buijs and Pasmans [34]. The roughness (Ra) was estimated using the kinetic energy predicted by the modified model as

$$Ra \approx \frac{0.63}{4}\left(\frac{3}{2\pi}\right)^{1/3}\left(\frac{E}{H}\right)^{1/2}\left(\frac{U}{H}\right)^{1/3}, \tag{6}$$

where $H(\mathrm{Pa})$, $E(\mathrm{Pa})$, and $K_{IC}(\mathrm{Pa\,m^{1/2}})$ are the target hardness, elastic modulus, and fracture toughness, respectively. U is the particle kinetic energy. According to the conservation of momentum and energy, the normal pressure also has a direct correlation with the kinetic energy. Therefore, the relationship between roughness and normal pressure can be established.

Based on the study and analysis of the microscopic physical process of abrasive impact the smooth surface in the previous literature, it is shown that the continuous impact of abrasive particles will lead to the removal of the material on the smooth surface and produce pits and defects. During the polishing process, the abrasive size is much larger than the size of the material surface topography. If the surface roughness is very low (smooth surface), this random removal process will increase the roughness with the increase of processing time. When the low-energy jet processes the surface for too long, pits and pores will be generated, the roughness will increase, and the surface quality will be reduced [27,28].

The exact relationship between roughness and kinetic energy has also been given in some relevant literature [33,34]. According to the momentum theorem, the kinetic energy of abrasive particle impact is directly proportional to the square of pressure, hence it can be explained that the change of roughness has a positive correlation with pressure. To simplify the physical problem and obtain the ideal model, this paper assumes the linear differential equation of the first order of pressure parameter to describe the surface roughness variation model over time, and the relationship between them is shown in Eq. (7). This model has a relatively concise form and accords with the previous analysis conclusions. The assumption will be verified by experiments.

$$\Delta Ra^{(i)} = C_1 p(x, y) \Delta t, \tag{7}$$

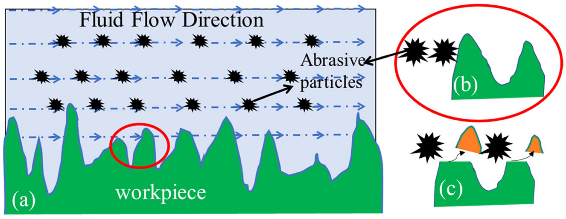

Fig. 6. Material removal model of the polishing area.

where $\Delta Ra^{(i)}$ is surface roughness variation under the influence of pressure, $p(x, y)$ is the normalization of normal pressure on the surface, Δt is the polishing time of change, and C_1 is the constant.

The impact process can actually be described as the effect of the fluid on the normal pressure on the surface, the distribution of which is a predictable position function that does not change with time, as shown in Fig. 3. On the surface of the workpiece in the impact area, materials form fragments and peel off, and the material removal is random. In the macroscopic expression, a small amount of material can be removed, which is why the removal rate of the impacting area is not zero in the actual polishing results. This random removal process on the workpiece surface has a low removal efficiency, but a great influence on the roughness.

B. Influence of the Shear Action on the Change in Roughness

In the polishing area, the material removal is mainly due to shear action. The tensile strength of the material is much lower than the compressive strength of the material. Therefore, when the fluid flows on the wall, the material removal rate is higher, and the removal depth increases linearly with the increase of polishing time. From the microremoval process, when the fluid flows through the surface of the workpiece, as shown in Figs. 6(a) and 6(b), the peak of the rough surface is cut by the abrasive at first, as shown in Fig. 6(c). The probability of abrasive contact with the valley part of the rough surface is very low, which is also the main reason why roughness can be reduced after polishing.

In the polishing process of surface microtopography, the peak value of the material is always preferentially removed. To accurately describe the influencing process of the wall jet on a rough surface, CFD simulation of the velocity distribution on a rough surface is performed, the initial parameters and boundary conditions are the same as the simulation in Section 2.B. The macroscopic rough surface diagram (with large value of roughness) is used to simulate the microscopic characteristics in Fig. 7.

Figure 7(a) shows that in the process of viscous fluid flow, because the surface is uneven, there is the Coanda effect [35], which causes a difference in velocity between the deep layer and the surface layer, and the surface peak velocity is greater than the valley velocity. From the perspective of material removal, the peak removal rate is high. Figure 7(b) is the pressure distribution of the fluid, and Fig. 7(c) is the shear force distribution of the abrasive to the rough surface. From the simulation results of the two, we draw the following conclusions: (1) in the flow direction, the force in front of the surface peak will be higher than that on the back, and there is a pressure difference on both sides, so there is a certain directionality in the removal of the material; and (2) the pressure and shear force are generally higher than the low-lying force, and the peak removal rate of the material removal is also high.

In the CFD simulation and relevant analysis as shown in this section, the conclusion is drawn that when the roughness is greater, the shear effect causes the roughness to decrease faster; however, when the roughness evaluation value is small, the influence of shear on the roughness evaluation has less impact. The shear effect on material removal is based on the Preston equation, which can be obtained by multiplying by shear velocity and pressure parameters. The current roughness value will also affect the change rate of roughness, that is, the change of roughness is positively correlated with the current roughness value. To simplify the physical problem and obtain the ideal model, this paper assumes the linear differential equation of the first order of three parameters to describe the surface roughness variation model over time, which is shown in Eq. (8). This model has a relatively concise form and accords with the previous analysis conclusions. Finally, the model will be verified by experimental results.

$$\Delta Ra^{(s)} = -C_2 p(x, y) v(x, y) Ra(t) \Delta t, \tag{8}$$

where $\Delta Ra^{(s)}$ is the surface roughness variation under the influence of shear, $v(x, y)$ and $p(x, y)$ are the normalization of fluid shear velocity and the stress at point (x, y) respectively, $Ra(t)$ is the roughness of the moment t, Δt is the polishing time of change, and C_2 is the constant.

C. Roughness Distribution Modeling

In the whole removal function at a point polishing, roughness has both the influence of pressure and the influence of shear. From Eqs. (7) and (8), it is concluded that pressure and shear have opposite effects on roughness variation. The combined action of the two causes the final roughness to have a certain distribution rule. In this section, the distribution of the roughness function will be deduced and solved.

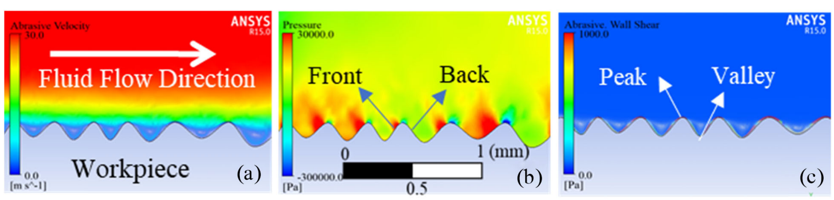

Fig. 7. Simulation of a rough surface between a fluid and the rough surface of (a) abrasive velocity, (b) pressure, and (c) abrasive wall shear.

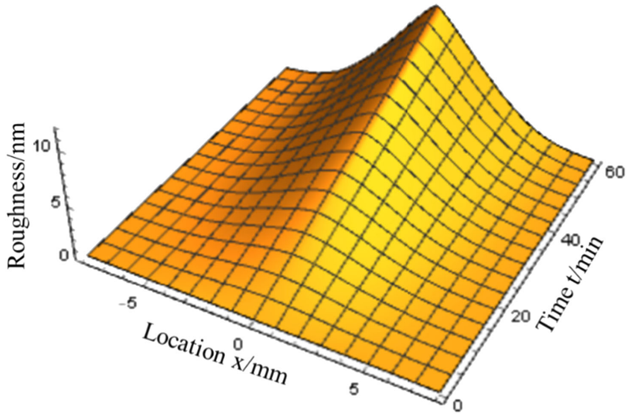

Fig. 8. Roughness distribution model over time.

The variation of the roughness can be described by Eq. (9), after adding Eqs. (7) and (8). By integrating Eq. (9) into Eq. (10), the relation of the roughness distribution of the final fixed-point removal function with time can be solved using Eq. (11).

$$\Delta Ra = \Delta Ra^{(i)} + \Delta Ra^{(s)} = C_1 p \Delta t - C_2 p v Ra(t) \Delta t, \quad \textbf{(9)}$$

$$\int \frac{dRa}{C_1 p - C_2 p v Ra(t)} = \int \mathrm{d}t, \quad \textbf{(10)}$$

$$Ra(x, y, t) = \begin{cases} \frac{C_1 - e^{-C_2 p(x,y) v(x,y)(t + C_3)}}{C_2 v(x,y)}, & \text{others} \\ Ra(x, y, t_0) + C_1 t, & \text{at point, } (0, 0) \end{cases}, \quad \textbf{(11)}$$

where ΔRa is the roughness variation of polishing for Δt at moment t, $Ra(x, y, t)$ is the roughness at point (x, y) when polishing for t at moment t_0, $Ra(x, y, t_0)$ is initial roughness at t_0, and C_1 and C_2 are constants. To meet the initial conditions such that when $t = 0$, $Ra(x, y, t) = Ra(x, y, t_0)$, C_3 is solved as follows:

$$C_3 = -\frac{\ln(C_1 - C_2 Ra(x, y, t_0) \cdot v(x, y))}{C_2 v(x, y)}. \quad \textbf{(12)}$$

Because the roughness distribution function model is a function of center rotation symmetry, the function can be described by reducing the dimension to two-dimensional space. The variation of the roughness distribution with position x and time is shown in Fig. 8. Only at the x = 0 position of the central region, roughness increases linearly with time. In other area, the roughness of the polishing area is a limited growth trend, of which the change in speed decreases gradually. Outside the removal function, although, there is fluid flowing at the surface; it does not change the initial roughness.

D. Modification of the Roughness Distribution Model

The roughness function model is based on the assumption of the shear velocity in the central area without value, and the calculation formula is Eq. (11). In the actual polishing process, as shown in Fig. 9(a), the jet beam has a certain width, and its influence on the surface roughness of the workpiece is regularly superposed. By convoluting the model with a rectangle function with width a in Eq. (13), we can obtain the smooth curve which is in agreement with the actual situation, as shown in the blue curve in Fig. 9(b). 'Without width' is ideal, a very thin jet beam. After polishing for a certain period of time, the roughness distribution of the removal function area shows a smooth Gaussian-like curve. The central region exhibits the maximum value of roughness, and the closer to the edge, the smaller the roughness.

$$Ra'(x, t_1) = Ra(x, t_1) * \mathrm{rect}(x/a), \quad \textbf{(13)}$$

where $Ra'(x, t_1)$ is the modified model at time t_1, $Ra(x, t_1)$ is the roughness distribution model in two-dimensional space at time t_1, '$*$' is the symbol of convolution, a is the nozzle width, and $\mathrm{rect}(x/a)$ is the rectangle function.

4. EXPERIMENTAL VERIFICATION

A. Experiment Setup and the Parameters

The MJP system, a portion of which is shown in Fig. 10(a), has been constructed using a six-degree-of-freedom robot. There is a mixing system, a delivery system, and a monitoring device inside the MJP platform. The MJP experiments were constructed using a six-degree-of-freedom robot, as shown in Fig. 10(b). The pressurization device was a single-screw pump that could be adjusted in the pressure range 0–2.2 MPa, at flow rates of 0–6 L/min. The specific parameters of the polishing processing are shown in Table 1. Through the numerical value of these

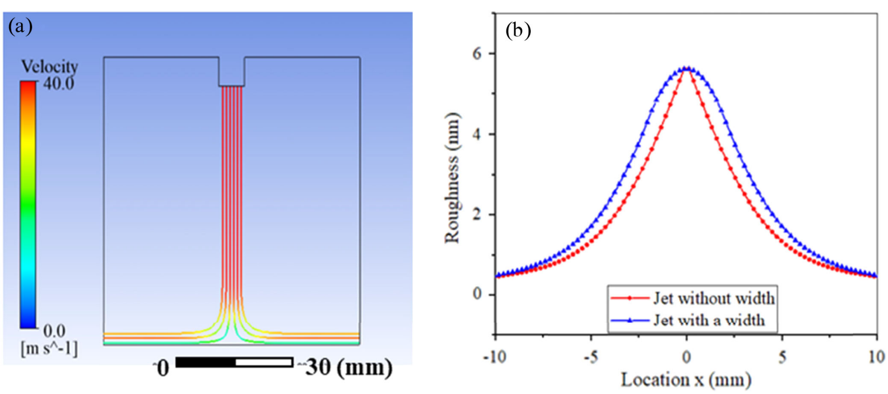

Fig. 9. (a) Fluid flow simulation with a width of 5 mm at a certain time, and (b) the effect of fluid jet width on the roughness distribution model.

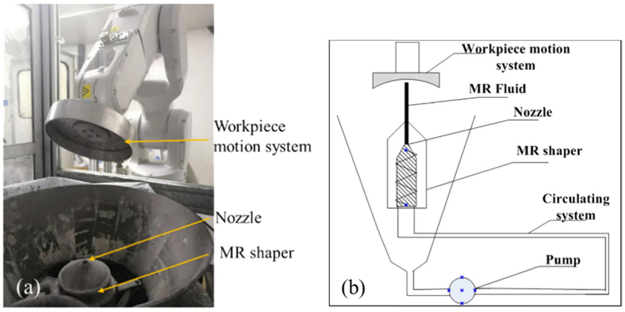

Fig. 10. MJP system with the robot; (a) photograph and (b) sketch.

Table 1. Parameters of the Polishing Process

Parameter	Value
Volume fraction of CeO_2 particles in fluid (%)	1
Diameter of CeO_2 particle (μm)	1
Volume fraction of Fe particle in fluid (%)	35
Diameter of Fe particle (μm)	1
Diameter of nozzle (mm)	5
Pressure (Mpa)	1
Magnetic strength (Gs)	120
Stand-off distance (mm)	50
Workpiece material	BK7

processing parameters, MJP can obtain a stable and accurate removal function.

The roughness function model discussed in Section 3.C is both a spatial distribution function and a time distribution function. To verify the correctness of the model, the following six experiments were performed at six different positions on the surface of the workpiece with the same initial roughness. Different experiments were conducted according to the experimental conditions in Table 2. The actual test results of the roughness are compared and verified with the model in the time domain and spatial domain. For polishing results with different polishing times, the roughness of each position was detected by a Zygo Newview 7200 white light interferometer, with RMS repeatability of less than 0.01 nm. The detection region of the white light interferometer is a rectangular region of 0.702 × 0.506 mm, and the initial roughness of the whole mirror is consistent, approximately 0.47 nm.

Table 2. Polishing Time with the MJP Tool at Different Fixed Points

Experiment	No	1	2	3	4	5	6
	Polishing time (min)	1	2	5	10	30	60
	Initial roughness (nm)	0.47 ± 0.03					

The removal function result tested by a Zygo interferometer of MJP on the fixed point polishing 60 s of a material surface is shown in Fig. 11, which is a removal model with a low center removal rate and a high surrounding removal rate. The comparison with other literature results proves the accuracy and universal applicability of the experimental equipment. In the next section, the roughness of each area of every removal function with different polishing times is tested. And the roughness value of the tested area is marked with black circles in Fig. 11 will make up distribution results and then be compared with the distribution model in Eq. (10).

B. Results of the Roughness Distribution in Time Domain

According to the theoretical model in Section 3.C, the roughness of different areas varies with time. To facilitate the analysis of the characteristics of the linear distribution in the central region, the mean values of several values in the central area are taken as the roughness values of the position $x = 0$ because it is difficult to accurately determine the roughness of the center point $x = 0$. The roughness of the polishing area and the central area of six removal functions, as shown in Fig. 4, was tested. The actual data in the central area selected are the average of several roughness results, and the standard deviation of the data calculated is expressed with error bars. The data selected in the polishing area are the average of the experimental data of several points approximately 3 mm away from the central area, and the standard deviation is expressed with error bars. The roughness results with error bars (standard error) are shown in Fig. 12.

The tested results in the central area are fitted linearly, and the linear equation is Eq. (11). The result of the coefficient of determination (R^2) is 0.9996, which shows that the straight line form of prediction of the roughness distribution in the central area is in good agreement, which can prove the correctness of the model in the central area. The roughness of the central area is only obtained by the integral of Eq. (7), without the participation of Eq. (8) ($C_2 = 0$). Therefore, the result of modified line

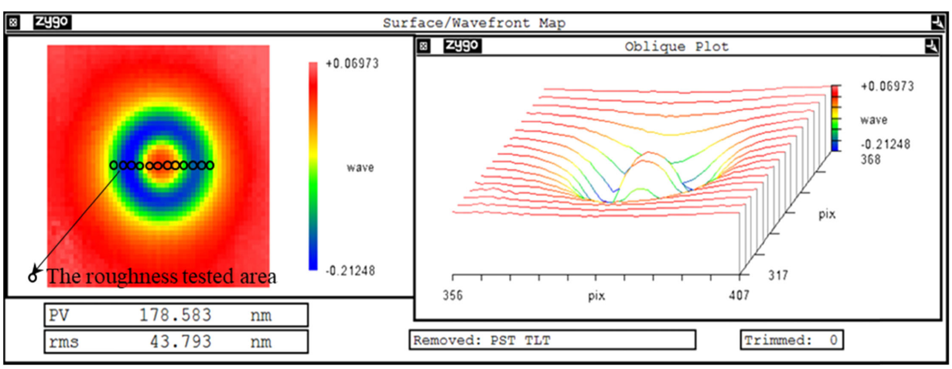

Fig. 11. Test result of the removal function on BK7 glass.

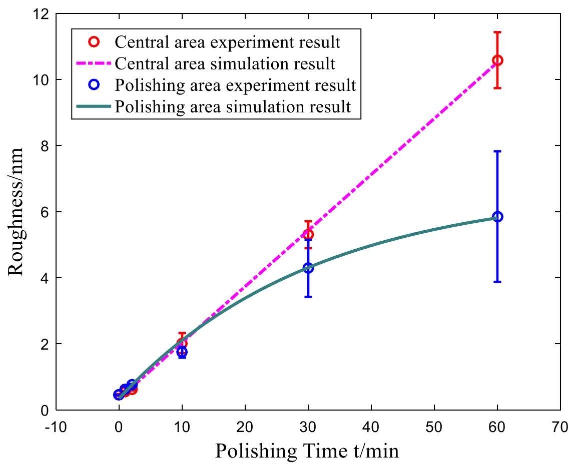

Fig. 12. Results of the experiment and simulation at different areas.

fitting also proves the correctness of the hypothesis of Eq. (7).

$$Ra(0, 0, t) = 0.349 + 0.169t, \tag{14}$$

where $Ra(0, 0, t)$ is the roughness in the central area for polishing t minutes.

The result of the polishing area, where $x = 3$, is evenly distributed on both sides of the curve drawn by Eq. (14), with parameters $C_1 = 0.169$, and $C_2 = 0.01$.

Ra is equal to 0.349 nm when t is 0, which is a bit smaller than the initial roughness in the actual polishing. Both the error of the measurement point selection and the error of timing within 1 s will affect the roughness measurement value. These are considered as fitting residuals, so the initial value error here of 0.1 nm can be accepted and ignored.

The experiment conducted at fixed points investigating the gradual change of the roughness distribution with time proves that the theoretical model is correct in the time domain.

With the increase of polishing time, the change in speed of the entire polishing area roughness is different. The central area roughness increases at a certain speed. The roughness of the polishing area exhibits a limited growth trend, of which the change in speed decreases gradually. Outside the removal function, although there is fluid flow, it does not affect the roughness.

In the time-domain evolution experiment, the experimental results have a good fit with the roughness distribution model, which proves the validity of the roughness distribution model of Eq. (11). Because the model of Eq. (11) is obtained by adding and integrating Eqs. (7) and (8), and the assumption of Eq. (7) has been proved correct by Eq. (14); it is concluded that the assumption of Eq. (8) is also correct.

C. Results of the Roughness Distribution in Spatial Domain

The roughness of 24 points with a blue marker was tested at equal intervals in the removal function region after polishing for 30 min, and the results of areas A, B, and C were used as examples in Figs. 13(a)–13(c). The roughness of 29 points with a red marker was tested at equal intervals in the removal function region after polishing for 60 min, and the results of areas D, E, and F were used as examples in Figs. 13(d)–13(f). The roughness distribution results for 30 and 60 min are shown in Fig. 13(g).

According to the test results of the 30 and 60 min fixed-point polishing, the roughness of the middle area is higher than that of the other areas, and the two sides are gradually reduced. Figs. 13(c)–13(e) show obvious pits and spots in the tested area, which are caused by the large normal pressure of the fluid in the central region of the surface. These pits and spots cause the surface roughness to increase and the surface quality to decrease.

Combined with the roughness models of Eqs. (10) and (12) in Sections 3.C and 3.D, when $Ra(x, y, t_0) = 0.349$ nm, $C_1 = 0.169$, and $C_2 = 0.01$, the roughness distribution curves of the 30 and 60 min polishing times are fitted, respectively. The roughness distribution curve drawn is in good agreement with the experimental results, which proves the correctness of the roughness distribution model. Similarly, this result also proves that the assumption in Sections 3.A and 3.B is correct.

The experiment conducted at fixed points investigating the gradual change of the roughness distribution with time proves that the theoretical model is correct in the spatial domain.

With the change of spatial position, the roughness distribution in the removal function is a kind of Gaussian-like distribution, with greater roughness in the central area and less roughness in the polishing region.

In the theoretical model, the initial roughness of the polished edge should be satisfied, but the edge position roughness of the area polished for 60 min is significantly higher than the initial roughness. The reason is that in the general research method, the pressure and velocity values selected in the model are truncated at the edge of the removal function. In the actual polishing process, the flow of fluid on the wall is continuous, and there is no cut-off. With the increase of polishing time, the radius of the removal area will increase. Therefore, the polishing radius in the 60-min treatment is different from that of the 30-min treatment. By modifying the edge of the pressure and velocity value, the fitting curve is more consistent with the experimental results.

D. Initial Condition of Roughness

In the model, if the initial roughness is larger than the limit value, the roughness of some polishing area will decrease. This experimental result is also consistent with the theoretical model. To verify that the roughness distribution of each point in the single-point removal function is inconsistent with the increase of time, polishing experiments according to the parameters in Table 3 are carried out to analyze the roughness variation function rule of the central area and polishing area under the parameters of Table 1.

When the initial roughness is larger than the limit of some area, it will decrease to the limit value. In Fig. 14, ‘x’ is the distance away from the central area. The blue lines are the simulation results from the roughness distribution model in Eq. (11).

The roughness of the polishing area and the central area of the three removal functions were tested. The actual data in the central area selected are the average of the experimental data of several points in the central area approximately 2 mm, and the standard deviation of the data calculated is expressed with

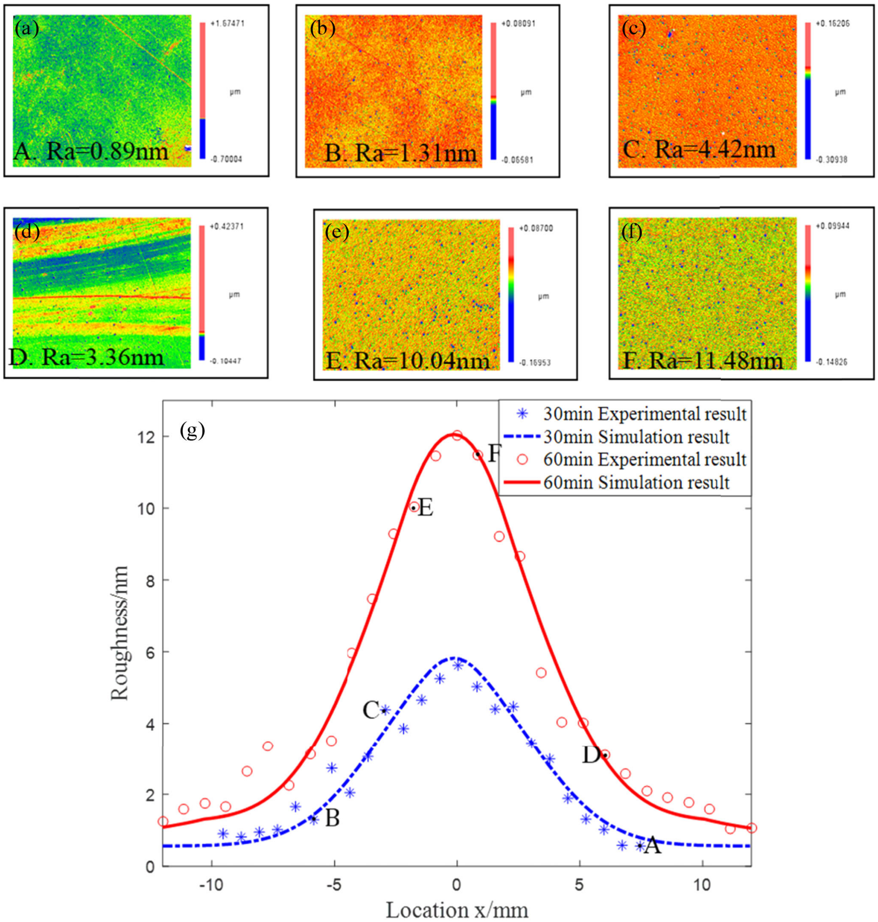

Fig. 13. Roughness distribution results in fixed point polishing for 30 min and 60 min, and different roughness from area A to area F.

Table 3. Polishing Time with MJP Tool in a Single Point

Experiment	No	1	2	3
	Polishing time (s)	60	120	300
	Initial roughness (nm)		1.2	

error bars. The data selected in the polishing area are the average of the experimental data of several points approximately 6 mm away from the central area, and the standard deviation is expressed with error bars. The roughness results with error bars (standard error) are shown in Fig. 14.

When the initial roughness is large, we obtain the conclusion from the surface roughness distribution model that different areas have different performance: some increases, and some decreases. In the central area, the value increased slowly at first and then fast. It is because when polishing time is short, the shearing effect is larger than the impacting effect. In the process of MR fluid vertical impact on the surface, the glass compressive strength (0.5–2 GPa) is large, and the initial pressure and energy are not enough to remove the material. However, the tensile strength of glass (30–85 MPa) is relatively small, and the fracture limit can be reached with only a small shear force to remove the material. When the fluid diffuses the surface, the sharp-angled abrasive particles can first perform a weak shear removal effect

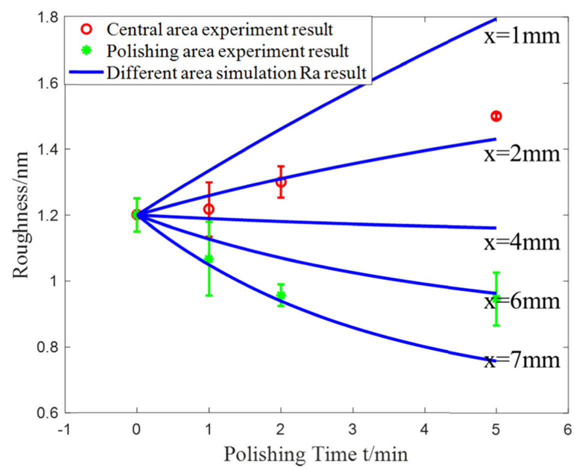

Fig. 14. Polishing and Impacting area Ra value with time.

on the material. Therefore, although the normal force is greater than the shear force, at this moment, the shearing effect on the material is greater than the impacting effect on the material. As the fluid constantly impacts on the surface, the impacting effect is greater than the shearing effect.

In the polishing area, the roughness decreased fast first and then slowly. We can get the limit roughness value which is

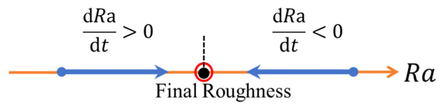

Fig. 15. Phase line of roughness in polishing area.

about 0.8 nm. So, if the initial roughness is larger than 0.8 nm, the roughness variation will be monotonic increasing; that is the reason of the result in Fig. 14 different from that in Fig. 13. And roughness in the central area will be larger than that in the area far away from the central area. The roughness variation of this process is consistent with the development trend of the model in Eq. (11).

The phase line of roughness changing with time is shown in Fig. 15, when the current roughness is larger than the limit value, and then the roughness decreases with time increasing, and the final roughness reaches a limit point. Otherwise, the final value will increase to the limit value like the result in Section 4.C.

5. CONCLUSIONS

In this paper, the surface roughness distribution model was established and verified. The paper starts with the basic theoretical model, in-depth study, and analysis of the reasons by CFD simulation, and finally put forward the surface roughness distribution model with time in the fixed removal function. The velocity and pressure in the MJP flow field are analyzed using a shear-stress transport $k-\omega$ model. The influence of velocity and pressure on the roughness change in the MJP process is studied, and the roughness distribution model in the removal function in the time domain and the spatial domain is established.

The experiment conducted at a certain point to investigate the gradual change of the roughness distribution with time proves that the theoretical model is correct to a certain extent. The roughness distribution of the removal function is complicated, and it is predictable that it changes with polishing time. The surface roughness at each area has a certain trend with polishing time. It can more clearly describe the variation rule of the roughness of each point, and improve the analytical model of roughness to better match the experimental results.

In this way, the roughness of the points in the single removal function area changes with the polishing time to form a roughness distribution model. This model can be analogized to the convolution of the removal function at whole-aperture polishing. As a similar convolution kernel, the model is finally used to analyze the roughness of each point after the whole-aperture polishing, to control the dwelling time per point, to design the step-size of polishing path on the workpiece, and finally maintain the roughness at a lower value. The surface distribution model is deemed to be more persuasive than the traditional roughness model, so the research has more important significance. The model laid a foundation, therefore, it has important guidance and reference value for the application to the whole aperture polishing.

Funding. National Natural Science Foundation of China (11903035, 61975201).

Disclosures. The authors declare no conflicts of interest.

REFERENCES

1. J. Tracy, W. Kordonski, A. Shorey, and M. Tricard, "Advances in finishing using magnetorheological (MR) jet technology," Proc. SPIE **10316**, 103160F (2007).
2. J. Seoka and Y. J. Kim, "A study on the fabrication of curved surfaces using magnetorheological fluid finishing," Int. J. Mach. Tools Manuf. **47**, 2077–2090 (2007).
3. M. Tricard, W. I. Kordonski, A. B. Shorey, and C. Evans, "Magnetorheological jet finishing of conformal, freeform and steep concave optics," CIRP Ann. **55**, 309–312 (2006).
4. W. I. Kordonski and A. B. Shorey, "Magnetorheological (MR) jet finishing technology," J. Intell. Mater. Syst. Struct. **18**, 1127–1130 (2007).
5. W. I. Kordonski, D. Golini, S. Hogan, and A. Sekeres, "System for abrasive jet shaping and polishing of a surface using magnetorheological fluid," U.S. patent US5971835A (October 26, 1999).
6. W. I. Kordonski, "Apparatus and method for abrasive jet finishing of deeply concave surfaces using magnetorheological fluid," U.S. patent US6561874 B1 (May 13, 2003).
7. W.-B. Kim, E. Nam, B.-K. Min, D.-S. Choi, T.-J. Je, and E.-C. Jeon, "Material removal of glass by magnetorheological fluid jet," Int. J. Precis. Eng. Manuf. **16**, 629–637 (2015).
8. K. Liu and S. N. Melkote, "Effect of plastic side flow on surface roughness in micro-turning process," Int. J. Mach. Tools Manuf. **46**, 1778–1785 (2006).
9. H. Wang, S. To, and C. Y. Chan, "Investigation on the influence of tool-tip vibration on surface roughness and its representative measurement in ultra-precision diamond turning," Int. J. Mach. Tools Manuf. **69**, 20–29 (2013).
10. W. Jingsi, Z. Jiaqi, and J. L. Pay, "Material removal in ultrasonic abrasive polishing of additive manufactured components," Appl. Sci. **9**, 5359 (2019).
11. N. Ikawa, R. R. Donaldson, R. Komanduri, W. König, T. H. Aachen, P. A. McKeown, T. Moriwaki, and I. F. Stowers, "Ultraprecision metal cutting—the past, the present and the future," CIRP Ann. **40**, 587–594 (1991).
12. T. Wang, H. Cheng, and H. Tam, "Mathematic models and material removal characteristics of multigesture jetting using magnetorheological fluid," Appl. Opt. **53**, 7804–7813 (2014).
13. T. Wang, H. Cheng, H. Yang, W. Wu, and H. Tam, "Controlling mid-spatial frequency errors in magnetorheological jet polishing with a simple vertical model," Appl. Opt. **54**, 6433 (2015).
14. Z. Xuecheng, D. Yifan, L. Shengyi, and P. Xiaoqiang, "Optimization of removal function for magnetorheological jet polishing," Proc. SPIE **6722**, 67221Y (2007).
15. T. Wang, H. B. Cheng, Z. C. Dong, and H. Y. Tam, "Removal character of vertical jet polishing with eccentric rotation motion using magnetorheological fluid," J. Mater. Process. Technol. **213**, 1532–1537 (2013).
16. H. Yang, H. Cheng, Y. Feng, and X. Jing, "Removal of millimeter-scale rolled edges using bevel-cut-like tool influence function in magnetorheological jet polishing," Appl. Opt. **57**, 3377–3384 (2018).
17. J. R. Haj Mohammad, J. K. Spelt, and M. Papini, "Surface roughness and erosion rate of abrasive jet micro-machined channels: experiments and analytical model," Wear **303**, 138–145 (2013).
18. D. Dehnadfar, J. Friedman, and M. Papini, "Laser shadowgraphy measurements of abrasive particle spatial, size and velocity distributions through micro-masks used in abrasive jet micro-machining," J. Mater. Process. Technol. **212**, 137–149 (2012).
19. T. Burzynski and M. Papini, "Analytical model of particle interference effects in divergent erosive jets," Tribol. Int. **43**, 554–567 (2010).
20. T. Burzynski and M. Papini, "Measurement of the particle spatial and velocity distributions in micro-abrasive jets," Measur. Sci. Technol. **22**, 025104 (2011).

21. S. Melle and J. E. Martin, "Chain model of a magnetorheological suspension in a rotating field," J. Chem. Phys. **118**, 9875–9881 (2003).
22. H. Yang, H. Cheng, H. Wu, and T. Wang, "Electromagnetic optimization of the integrated magnetorheological jet polishing tool and its application in millimeter-scale discontinuous structure processing," Appl. Opt. **56**, 3162–3170 (2017).
23. Z. Zhang and C. Kleinstreuer, "Low Reynolds number turbulent flows in locally constricted conduits," AIAA J. **41**, 831–840 (2003).
24. Y. Yu, X. Liu, J. Wu, and H. Meng, "Comparison among turbulence models for a novel static circulating jet mixer," Appl. Mech. Mater. **28**, 382–385 (2010).
25. H. Liu, J. Wang, N. Kelson, and R. J. Brown, "A study of abrasive waterjet characteristics by CFD simulation," J. Mater. Process. Technol. **153**, 488–493 (2004).
26. C. Y. Shi, J. H. Yuan, and F. Wu, "Analysis of parameters in fluid jet polishing by CFD," Proc. SPIE **7282**, 72821Y (2009).
27. F. Frost, R. Fechner, B. Ziberi, D. Flamm, and A. Schindler, "Large area smoothing of optical surfaces by low-energy ion beams," Thin Solid Films **459**, 100–105 (2004).
28. A. Schindler, T. Haensel, D. Flamm, W. Frank, G. Boehm, F. Frost, R. Fechner, F. Bigl, and B. Rauschenbach, "Ion beam and plasma jet etching for optical component fabrication," Proc. SPIE **4440**, 217–227 (2001).
29. S. K. Paswan, T. S. Bedi, and A. K. Singh, "Modeling and simulation of surface roughness in magnetorheological fluid based honing process," Wear **376-377**, 1207–1221 (2017).
30. S. Jha and Z. Alam, "Modeling of surface roughness in ball end magnetorheological finishing (BEMRF) process," Wear **376-377**, 194–202 (2017).
31. E. Ness and R. Zibbell, "Abrasion and erosion of hard materials related to wear in the abrasive waterjet," Wear **196**, 120–125 (1996).
32. S. M. Booij, "Fluid jet polishing: possibilities and limitations of a new fabrication technique, Ph.D. Thesis (Technical University of Delft Netherlands, 2003).
33. P. J. Slikkerveer, P. C. P. Bouten, F. H. Veld, and H. Scholten, "Erosion and damage by sharp particles," Wear **217**, 237–250 (1998).
34. M. Buijs and J. M. M. Pasmans, "Erosion of glass by alumina particles: transitions and exponents," Wear **184**, 61–65 (1995).
35. T. Panitz and D. T. Wasan, "Flow attachment to solid surfaces: the Coanda effect," AIChE J. **18**, 51–57 (1972).